Available online at www.sciencedirect.com
SCIENCE DIRECT®
PERGAMON
International Journal of Heat and Mass Transfer 46 (2003) 4629–4638
International Journal of HEAT and MASS TRANSFER
www.elsevier.com/locate/ijhmt

Turbulent convection of air-cooled rectangular duct with surface-mounted cross-ribs

T.T. Wong [a], C.W. Leung [a,*], Z.Y. Li [b], W.Q. Tao [b]

[a] Department of Mechanical Engineering, The Hong Kong Polytechnic University, Hung Hom, Kowloon, Hong Kong
[b] School of Power and Energy Engineering, Xi'an Jiaotong University, Xi'an, China

Received 12 June 2002; received in revised form 29 May 2003

Abstract

Experimental and numerical studies were conducted to investigate the forced convection and flow friction of a turbulent airflow in a horizontal air-cooled rectangular duct, with square-sectioned cross-ribs mounted on its bottom surface. Cross-sectional dimensions of the cross-ribs were 6.37 mm × 6.37 mm. Reynolds number of the fully turbulent flow was maintained constant at 12,380. Heat was supplied uniformly to the airflow via bottom surface of the duct only. Effects of varying the angle formed by the cross-ribs between 30° and 120° on the forced convection and flow friction were studied. It was found that an optimum angle corresponding to the highest heat transfer coefficient occurred between 60° and 70°.

Computational predictions of forced convection and flow friction of the same rectangular duct mounted with cross-ribs were performed with the zonal k–ε model, the stability-guaranteed second-order difference scheme and the block implicit method. A comparison with the experimental results indicated that a reasonably good agreement had been achieved. Existence of an optimum angle formed by the cross-ribs between 60° and 70° was also indicated, except the numerical predictions were lower than the experimental findings by approximately 2–10%. However, the flow friction had been slightly over-estimated by 2–11% with the numerical model.

It was shown that forced convection could be enhanced sufficiently by mounting cross-ribs on the internal surfaces of a rectangular duct, especially when the optimum angle was used.

Keywords: Forced convection enhancement; Turbulent heat transfer; Rectangular duct with cross-ribs; Zonal k–ε model: SGSD and BIM

1. Introduction

Artificial roughness on a surface has been widely accepted as an effective technique to enhance the heat transfer rate in a heat exchanger or the cooling passage of a gas turbine blade. Roughness elements are used to improve the convective heat transfer by promoting local turbulence in the flow, however, it also leads to an increase in pressure loss and hence a greater forced draught will be required. In order to keep the pressure loss at a low level the turbulence should be created essentially in the region very close to the surface, namely, the laminar sub-layer. Consequently, roughness elements or grooves are usually produced on the internal surfaces of a duct by appropriate machine processes or attachment of small ribs.

A number of investigations had been carried out on the heat transfer characteristics of rectangular ducts with parallel ribs placed at right angle to the main flow direction, and the ribs were made of different cross-sections. Han [1] investigated experimentally the forced convection in channels with parallel and crossed V-shaped ribs. Liou and Hwang [2] studied experimentally

* Corresponding author. Tel.: +852-2766-6651; fax: +852-2365-4703.
E-mail address: mmcwl@polyu.edu.hk (C.W. Leung).

0017-9310/$ - see front matter © 2003 Elsevier Ltd. All rights reserved.
doi:10.1016/S0017-9310(03)00298-9

Nomenclature

A	surface area of the bottom surface of the test section (m^2)
a	coefficients of the discretized Momentum Equations (kg/s)
b	constant source term
C_1, C_2, C_3	numerical constants in Eqs. (5)–(7)
D	interface diffusive flux (m/s)
e	the rib dimension (or height) (m)
D_e	equivalent hydraulic diameter of the test section (m)
E, W, N, S	locations of the eastern, western, northern and southern points of the control volume
e, w, n, s	locations of the eastern, western, northern and southern interfaces of the control volume
$\dot{E}$	electric power supply to the heating plate (W)
f	average friction factor as defined in Eq. (2)
h_m	average convective heat transfer coefficient ($W/m^2\,K$)
L	length of the test section (m)
m, n, p	power index in Eqs. (5)–(7)
Nu_{D_e}	average Nusselt number as defined in Eq. (1)
Pr	Prandtl number
$\dot{Q}$	forced convection to the airflow (W)
Re_{D_e}	Reynolds number $\left[=\frac{u_m D_e}{v}\right]$
S	source term
T_{fm}	average fluid temperature in the test section (K)
T_{wm}	average wall temperature of the test section (K)
u, v, w	velocity component (m/s)
u_m	mean velocity through the test section (m/s)
x, y, z	Cartesian ordinates (m)
Γ	effective diffusive coefficient
ϕ	general variable
v	kinetic viscosity of the airflow (m^2/s)
θ	angle formed by the cross-ribs (deg)
λ	thermal conductivity of the airflow (W/m K)
ρ	density of the airflow (kg/m^3)
Δp	pressure drop across the test section (N/m^2)

the turbulent heat transfer and flow friction characteristics in a rectangular channel mounted with parallel triangular, semi-circular and square ribs on its internal walls. Thermal performance of the slit-ribbed channel had also been investigated [3] and was compared with that of the solid-ribbed channel. Lorenz et al. [4] measured the distribution of convective heat transfer coefficient and pressure drop along the wall of a parallel-ribbed channel by means of infrared thermograph. Hwashida [5] studied experimentally the local heat transfer of a parallel-ribbed surface with air at atmospheric pressure and room temperature as the working fluid. Saini and Saini [6] investigated the effect of using an expanded metal mesh to produce roughness on the convective heat transfer coefficient and friction factor of a turbulent flow in a rectangular duct with large aspect ratio. Chandra et al. [7] carried out an investigation on the effect of adopting circular-rib and square-rib profiles on turbulent channel flow heat transfer and flow friction characteristics. Wang et al. [8] conducted a study on the heat transfer of a developing turbulent flow in a ribbed convergent/divergent square duct. Wong and Leung [9,10] compared the thermal performance of air-cooled triangular ducts fabricated with several kinds of artificially roughened surfaces. Internal roughness was produced on the internal surface of a triangular duct by machine processes or fixing parallel square ribs/V-grooves. It was concluded that the ribbed surface was able to produce the highest heat enhancement.

The previous results were obtained primarily for parallel ribs lying normally to the main airflow direction, and mounting on one or two principal walls of the duct. However, orthogonal to the main flow might not necessary be the best arrangement to position the ribs [6], and properly designed cross-ribs had been suggested to provide even better thermal performance. Han et al. [11] found that ribs inclining at an angle of attack of 45° were able to produce superior heat transfer performance. The present study was therefore carried out to investigate the feasibility of using cross-ribs to enhance the forced convection in a rectangular duct. Effect of changing the angle formed by the cross-ribs (θ) on the convective heat transfer coefficient and friction factor of the turbulent airflow in a rectangular duct were studied by maintaining the Reynolds number constantly at 12,380. Cross-ribs of uniform cross-sectional dimension were mounted on bottom surface of the duct. For comparison purpose, thermal performance of the same rectangular duct with smooth internal surfaces was also investigated. Investigations on the heat transfer performance of turbulent flow in cross-ribbed ducts, especially numerically, have rarely been reported. Therefore numerical study of the forced convection in cross-ribbed rectangular duct was also conducted in the present

work, in order to provide a better understanding of its heat transfer characteristics.

2. Experimental arrangement

2.1. Test apparatus

In the present experimental study, the rectangular duct consisted of an entrance section of 1000 mm length, a test section of 1000 mm length, a combination section of 400 mm length and an exit section of 1400 mm length, as shown in Fig. 1. The first three sections, having identical cross-sectional shape and dimensions of 150 mm width and 30 mm height, were fabricated with wooden plates of 18 mm thickness. They were joined together with flanges consisting of a wooden plate, a duralumin plate and a rubber sheet in sandwich arrangement. The entrance section had a hydraulic diameter of 50 mm and a sufficiently long length of 1000 mm to ensure a fully-developed flow in a significant part of the test section under turbulent flow condition [9,10]. The wooden plate and the rubber sheet served as thermal insulation to avoid heat loss from the ends of the test section to the entrance and combination sections. The combination section and the exit section were thermally insulated by a 40 mm thick glass fiber blanket with thermal conductivity of 0.35 W/m K to minimize the heat loss.

A cross-sectional view of the test section is shown in Fig. 2. Bottom surface of the test duct consisted of three layers arranging in sandwich: a duralumin plate of 2 mm thickness, a heating plate of 2 mm thickness and a wooden plate of 18 mm thickness. A thin duralumin plate of high thermal conductivity of 180 W/m K was

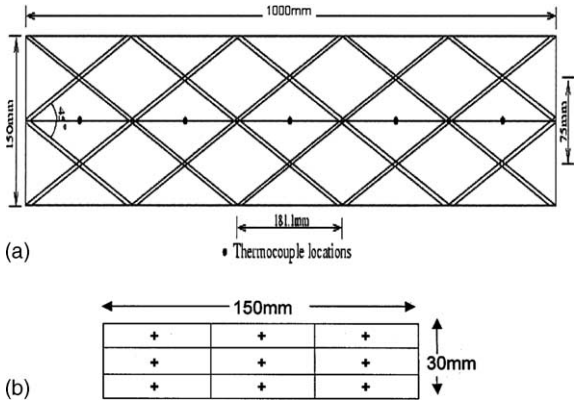

Fig. 2. (a) Thermocouple locations along the test duct. (b) Area-averaged pressure measurement locations.

used to achieve a more uniform heat flux to the airflow. Each duralumin square rib was attached to the duralumin plate by means of two M1-screws according to a pre-determined crossing-pattern, and an aluminium foil of 0.18 mm thickness was applied between the ribs and the duralumin plate to ensure an excellent and uniform contact. The solid square ribs used in the present investigation had a uniform cross-sectional dimension of 6.37 mm × 6.37 mm. The rib height to channel hydraulic diameter ratio was 0.127. The rib height chosen was to ensure that it would be greater than the laminar sublayer thickness even at low Reynolds number [9,10]. A thick wooden plate was used to provide a high resistance to the heat flow such that most of the heat generated by the heating plate could be delivered to the airflow via the duralumin plate. Arrangement of the cross-ribs on the bottom surface is presented in Fig. 2a for the case of an

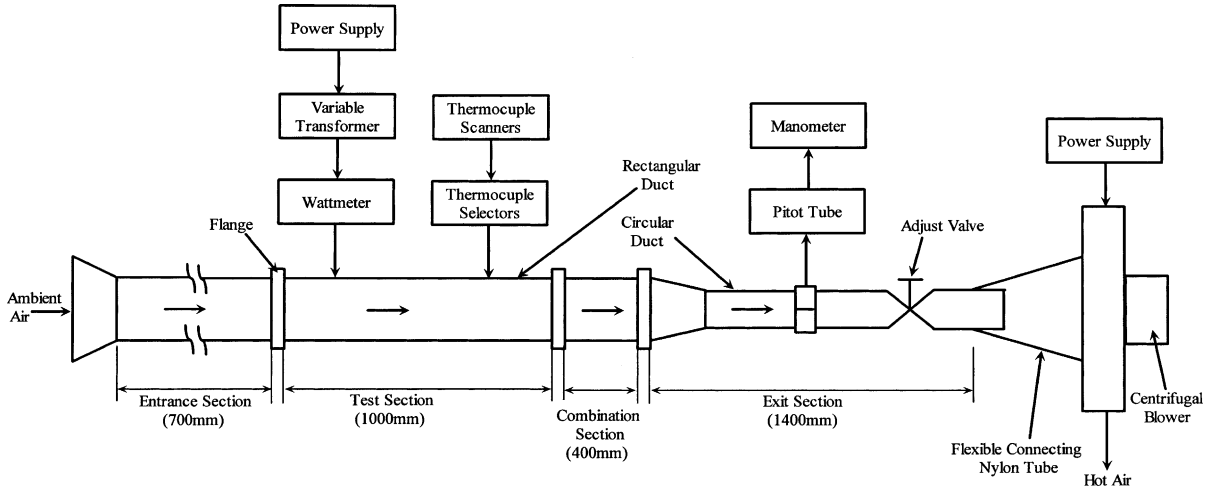

Fig. 1. Experimental set-up.

angle of 45° formed by the cross-ribs. Centerline through the crossing point of two ribs was in the axial direction of the duct. There were three centerlines across the width of the duct, with one at the middle and the other two along the two edges. Other angles between 30° and 120° had also been used in the present study with an interval of 10°. When the angle increased, separation between two consecutive crossing points along the axial direction of the duct decreased.

The combination duct was designed to ensure a more accurate measurement of the exit air temperature [12]. In order to measure the bulk temperature of heated fluid more accurately, a special mixing device had been built inside the combination duct, which consisted of two specially fabricated plates installing at a right angle to the main flow direction and separating by an axial distance of 200 mm. The first plate had a bigger rectangular hole of 200 mm × 20 mm at its center, while the second plate possessed eight smaller circular holes of 14 mm diameter. When the air stream was flowing through these two specially fabricated plates, strong mixing was occurred leading to a more uniform temperature of the exit flow.

A centrifugal blower powered by a 1.5 kW electric motor drove the ambient air through the rectangular duct, and the mass flow rate could be controlled by the air adjust-valve, which was fixed at the exit of the exit section. A FC501 micro-manometer equipped with a Pitot tube, two digital thermometers and a Pitot tube were the major instruments used to measure pressure, temperature and mass flow rate respectively. Uniform heating was provided by the electrically heating plate, which was fixed between the duralumin plate and the wooden plate at the bottom surface of the test duct with connecting bolts. The heating plate was able to supply a maximum power of 1800 W, which was measured by a power-meter and regulated by a variable transformer.

The same test apparatus was used for the experiments conducted with the rectangular duct of smooth internal surfaces, during which no ribs were attached.

2.2. Measurement of temperature, pressure drop and flow rate

2.2.1. Temperature measurement

The inlet air temperature was measured by a T-type thermocouple positioned at the inlet of the entrance duct. There were five T-type thermocouples used to measure the outlet air temperature. These thermocouples were placed on a very thin duralumin mesh connecting to the flange between the combination duct and the exit duct. Wall temperatures of the test duct were measured with T-type thermocouples. Locations of the thermocouples were varied in different tests, depending on the angle formed by the cross-ribs on the duralumin plate. As shown in Fig. 2a, five thermocouples were embedded at the center of each parallelogram along the centerline of the duct. In order to install the thermocouples, small holes and shallow grooves were machined on the backside of the duralumin plate. Each of these grooves was 1 mm deep and 1 mm wide, being vertical to the axial centerline of the duralumin plate. A small hole of 1 mm depth and 0.6 mm diameter was drilled at the end of each shallow groove. The junction of each thermocouple was then affixed to the small hole with soldering tin and epoxy. Epoxy was also applied to the shallow groove to hold the thermocouple in place. Good physical contact between the thermocouple and the small groove was checked with a multi-meter. The error in temperature measurement should be within ±0.5 °C.

2.2.2. Pressure drop measurement

In order to determine the pressure drop across the test section, the area-averaged pressures at two cross-sectional planes in the test section were obtained. Both planes were 0.2 m from both ends of the test duct, where the end effect, which was further minimized together with the use of the entrance and exit ducts, became negligible. At each plane, nine pressure measurements were made using a Pitot tube, which was inserted into the test section through the three circular pressure taps at its top wall with the vertical position fixed by means of a vernier. The measurement points were the centers of a uniform 3 by 3 array of rectangles with each of them having a dimension of 50 mm width and 10 mm height. The taps were fabricated with organic glass and each of them had a diameter of 1.5 mm. An FC501 micro-manometer was used to provide the pressure readings from the Pitot tube signals in the range from 2 to 200 Pa with an error on the reading of ±1%.

2.2.3. Measurement of flow rate

The air velocity distribution across the duct was measured with a Pitot tube of 5 mm diameter, which was fixed at the exit section and equipped with a manometer. An adjust-valve was installed at the inlet of the blower to control the flow rate of air through the system as shown in Fig. 1. The local air velocities were taken from nine different locations with an interval of 5 mm across the same cross-sectional plan of the exit. Accurate positioning of the Pitot tube was achieved by using a vertical traversing mechanism mounted on a vernier caliper. The airflow rate was then obtained by numerical integration over the cross-section. The error in flow rate measurement by using this method should be within ±4% [9,10].

2.2.4. Measurement of time-averaged experimental data

Because of the highly transient nature of a turbulent flow, a personal computer was used to facilitate the measurement of experimental data as presented in the previous study of Wong and Leung [9,10]. Recording of the data was started only when the entire system had

achieved its steady-state after running for a certain period. Data would be taken continuously for 1 min with a sampling time of 1 s. This period should not be too long to avoid significant change of the operating conditions. The recorded data were then examined to ensure no large deviation was existed, before they were averaged to give the time-averaged experimental values.

3. Data processing and handling

The experimental data were rearranged into non-dimensional parameters. The average Nusselt number and friction factor of the duct were defined as:

$$Nu_{D_e} = \frac{h_m D_e}{\lambda} \tag{1}$$

$$f = \frac{\left(\frac{\Delta p}{L}\right) D_e}{\frac{1}{2}\rho u_m^2} \tag{2}$$

Hydraulic diameter of the test section (D_e) was maintained constantly at 0.05 m throughout the present study.

The average heat transfer coefficient of the bottom surface of the rectangular duct was determined by:

$$h_m = \frac{\dot{Q}}{A(T_{wm} - T_{fm})} \tag{3}$$

In the determination of the heat transfer to the airflow by forced convection ($\dot{Q}$), heat loss via external surfaces and ends of the test section was first deducted from the power supply ($\dot{E}$) to the heating plate. Using the same procedure as adopted in a previous study of Wong and Leung [9,10], this heat loss was predicted to be around 8% of the power supply, i.e.

$$\dot{Q} = 0.92\dot{E} \tag{4}$$

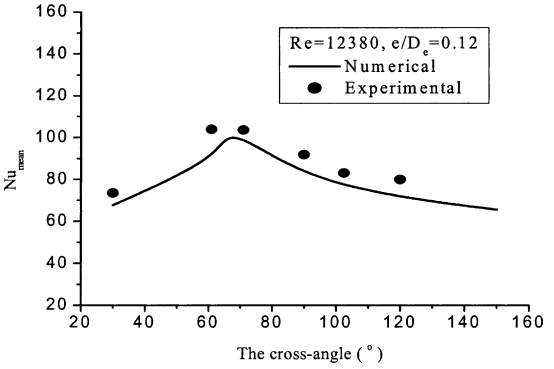

Fig. 3. Variation of average Nusselt number with cross-rib angles.

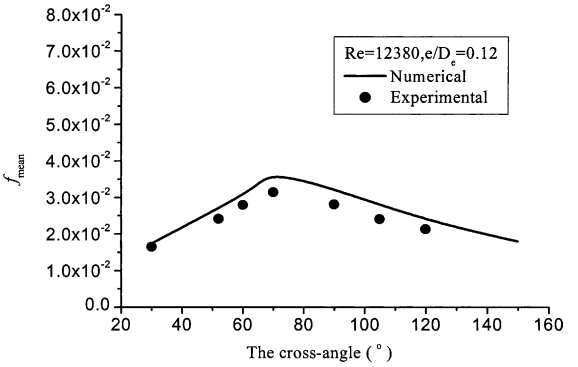

Fig. 4. Variation of average friction factor with cross-rib angles.

Because of the very low temperature variation between internal surfaces of the test section and the absence of absorbing gas, radiation could be assumed negligible [9,10]. The average Nusselt number and friction factor of the rectangular duct calculated from Eqs. (1) and (2) were plotted against angle formed by the cross-ribs, and presented in Figs. 3 and 4 respectively.

4. Numerical simulation

4.1. Mean flow equations

In the present study, numerical simulations were performed for the above-mentioned rectangular duct using the zonal k–ε model and the block implicit method (BIM). The zonal k–ε model comprises a combination of the high-Re k–ε model for the fully turbulent core and the low-Re one-equation-model of the k-transport equation, in which the dissipation rate, ε, within the near-wall region is obtained from the near-wall distance. The model has been applied with reasonable success to the computation of heat transfer in two-dimensional ribbed passage [13]. The coordinate system used for the present study is shown in Fig. 5a. The governing equations are expressed in Cartesian tensor notation as follows:

Continuity:

$$\frac{\partial(\rho u_j)}{\partial x_j} = 0 \tag{5}$$

Momentum transport:

$$\frac{\partial(\rho u_j u_i)}{\partial x_j} = -\frac{\partial p}{\partial x_i} + \frac{\partial}{\partial x_j}\left[\mu\left(\frac{\partial u_i}{\partial x_j} + \frac{\partial u_j}{\partial x_i}\right) - \rho\overline{u_i' u_j'}\right] \tag{6}$$

Energy:

$$\frac{\partial(\rho u_j T)}{\partial x_j} = \frac{\partial}{\partial x_j}\left[\frac{\mu}{Pr}\frac{\partial T}{\partial x_j} - \rho\overline{u_j' T'}\right] \tag{7}$$

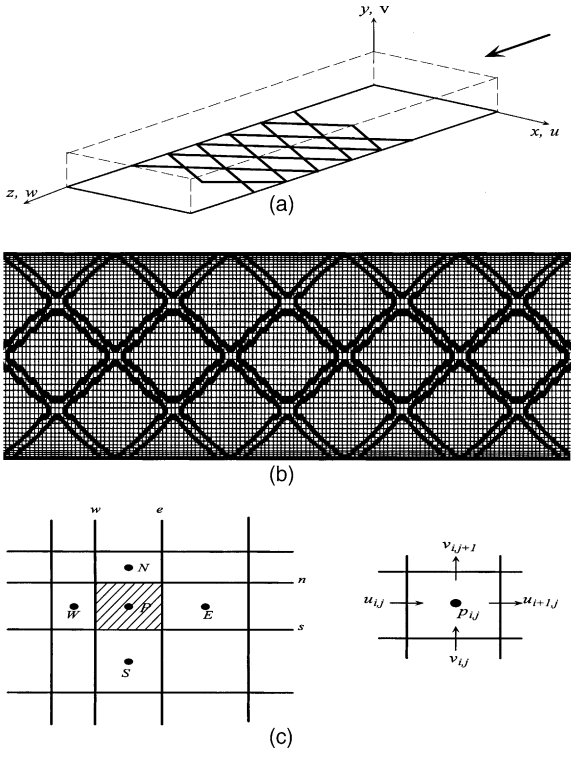

Fig. 5. (a) Coordinate system used for the present study. (b) Computational grid (cross-rib angle = 60°). (c) The control volume "P".

4.2. Turbulence modeling equations

Effective viscosity model (EVM) [13]:

$$-\rho\overline{u_i'u_j'} = -\frac{2}{3}k\delta_{ij} + \mu_t\left(\frac{\partial u_i}{\partial x_j} + \frac{\partial u_j}{\partial x_i}\right), \quad \mu_t = \rho c_\mu \frac{k^2}{\varepsilon} \tag{8}$$

In the fully turbulent core:

$$\frac{\partial(\rho u_j k)}{\partial x_j} = \frac{\partial}{\partial x_j}\left[\left(\mu + \frac{\mu_t}{\sigma_k}\right)\frac{\partial k}{\partial x_j}\right] + P_k - \rho\varepsilon \tag{9}$$

$$P_k = -\rho\overline{u_i'u_j'}\left(\frac{\partial u_i}{\partial x_j}\right) \tag{10}$$

$$\frac{\partial(\rho u_j \varepsilon)}{\partial x_j} = \frac{\partial}{\partial x_j}\left[\left(\mu + \frac{\mu_t}{\sigma_\varepsilon}\right)\frac{\partial \varepsilon}{\partial x_j}\right] + \frac{\varepsilon}{k}(c_{\varepsilon 1}P_k - \rho c_{\varepsilon 2}\varepsilon) \tag{11}$$

In the near-wall region [14], the dissipation rate and the turbulent viscosity were obtained from:

$$\varepsilon = \frac{k^{3/2}}{l_\varepsilon} \quad \text{and} \quad \mu_t = \rho c_\mu l_\mu \sqrt{k} \tag{12}$$

The length scales were obtained from the near-wall distance, Y, according to:

$$l_\varepsilon = 2.55Y[1 - \exp(-0.263y^+)] \tag{13}$$

$$l_k = 2.55Y[1 - \exp(-0.016y^+)] \tag{14}$$

where $y^+ = \rho\sqrt{k}Y/\mu$ is the dimensionless wall distance.

4.3. Modeling of turbulent heat fluxes

The effective diffusivity approximation was employed for the heat fluxes.

$$-\rho\overline{u_i'T'} = \frac{\mu_t}{\sigma_T}\frac{\partial T}{\partial x_i} \tag{15}$$

4.4. Modeling constants

The empirical constants in the turbulence equations have the following values, in accordance with the proposals of Jones and Launder [13] for the k and ε equations:

c_μ	$c_{\varepsilon 1}$	$c_{\varepsilon 2}$	σ_k	σ_ε	σ_T
0.09	1.44	1.92	1	1.3	0.9

5. Computational details

In this section, the grid system, numerical algorithm and the difference scheme of the convection term are described briefly.

5.1. The present grid

The domain extension method was adopted. In this method, a stair-stepped boundary was used to simulate the curve or skew geometric boundary. Such treatment may cause some errors which can be eliminated by refining the grid. Moreover, the fluid–solid coupled heat transfer can be solved better using this method [15]. The present computational grid of $52\times32\times132$ is shown in Fig. 5b, which becomes finer near the solid walls. The effect of the grid spacing on the computed results was checked by increasing the grid number to $102\times62\times132$, and no obvious difference for both the friction factor and Nusselt number was observed.

5.2. Discretization of the governing equations

The differential equations in respect of a variable ϕ for a steady-state convection–diffusion problem can be written as:

$$\frac{\partial(\rho u_j \phi)}{\partial x_j} = \frac{\partial}{\partial x_j}\left(\Gamma_\phi \frac{\partial \phi}{\partial x_j}\right) + S_\phi \tag{16}$$

A two-dimensional problem is taken as an example for demonstration purpose. The typical control volume is shown in Fig. 5c. The finite-volume method is applied. Therefore, after integrating over the control volume P, the discrete equation becomes:

$$F_e\phi_e - F_w\phi_w + F_n\phi_n - F_s\phi_s = S_\phi \delta x\,\delta y + D_e(\phi_E - \phi_P) - D_w(\phi_W - \phi_P) + D_n(\phi_N - \phi_P) - D_s(\phi_S - \phi_P) \quad (17)$$

The variable ϕ at the control volume interface can be determined using an interpolation or extrapolation involving values of the geometric shape of the neighboring grid-point.

To complete the discretization process, the interface values of ϕ are interpolated by the stability-guaranteed second-order difference (SGSD) scheme [16]. This scheme can automatically choose the appropriate difference scheme according to the available local field information in different space and/or time. It automatically approaches the central difference scheme where or when the diffusion is dominant, and approaches the second-order upwind difference scheme where or when the convection is dominant. It is a scheme that demonstrates absolute stability and high accuracy. For example, the value of variable ϕ on the east surface is estimated as:

$$\phi_e = \beta\phi_e^{CD} + (1-\beta)\phi_e^{SUD} \quad \text{and} \quad \beta = 2/(2+|P_\Delta|) \quad (18)$$

CD and SUD designate the central difference and the second-order upwind difference. The factor β is obtained from the previous iteration results and P_Δ is Peclet number of the grid. For stable convergence during the iteration procedures, the deferred-correction method is adopted, which is initially proposed in [17] and latter enhanced in [18]. With the deferred-correction method, interpolation for the interface variable is expressed as the sum of a low-order (such as the first-order upwind) difference scheme and a correction term corresponding to the scheme is employed. Thus Eq. (18) may be written as:

$$\phi_e = \phi_e^{FUD} + \{[\beta\phi_e^{CD} + (1-\beta)\phi_e^{SUD}] - \phi_e^{FUD}\}^{old} \quad (19)$$

FUD designates the first-order upwind difference and *old* designates the previous iteration results. Using Patankar's notation [19], Eq. (17) can be written in the form:

$$a_P\phi_P = a_E\phi_E + a_W\phi_W + a_N\phi_N + a_S\phi_S + b + S_{ad} \quad (20)$$

where $a_P = a_E + a_W + a_N + a_S - S_P\delta x\,\delta y$

$a_E = D_e + [|-F_e, 0|]$

$a_W = D_w + [|F_w, 0|]$

$a_N = D_n + [|-F_n, 0|]$

$a_S = D_s + [|F_s, 0|]$

$b = S_c\delta x\,\delta y$

$S_{ad} = -S_{ad,e} + S_{ad,w} - S_{ad,n} + S_{ad,s}$

S_{ad} is the additional source term because of employing the deferred-correction method.

5.3. Block implicit method [20]

For the four interfaces of the control volume P denoted by (i,j), we have:

$$A_c^u u_{i,j} = A_W^u u_{i-1,j} + A_E^u u_{i+1,j} + A_S^u u_{i,j-1} + A_N^u u_{i,j+1} + (p_{i-1,j} - p_{i,j})\delta y + (S^u\delta x\,\delta y + S_{ad}^u)_{i,j} \quad (21)$$

and

$$A_c^u u_{i+1,j} = A_W^u u_{i,j} + A_E^u u_{i+2,j} + A_S^u u_{i+1,j-1} + A_N^u u_{i+1,j+1} + (p_{i,j} - p_{i+1,j})\delta y + (S^u\delta x\,\delta y + S_{ad}^u)_{i+1,j} \quad (22)$$

and

$$A_c^v v_{i,j} = A_W^v v_{i-1,j} + A_E^v v_{i+1,j} + A_S^v v_{i,j-1} + A_N^v v_{i,j+1} + (p_{i,j-1} - p_{i,j})\delta x + (S^v\delta x\,\delta y + S_{ad}^v)_{i,j} \quad (23)$$

and

$$A_c^v v_{i,j+1} = A_W^v v_{i-1,j+1} + A_E^v v_{i+1,j+1} + A_S^v v_{i,j} + A_N^v v_{i,j+2} + (p_{i,j} - p_{i,j+1})\delta x + (S^v\delta x\,\delta y + S_{ad}^v)_{i,j+1} \quad (24)$$

The continuity equation can be approximated by central difference scheme:

$$(\rho u_{i+1,j} - \rho u_{i,j})\delta y + (\rho v_{i,j+1} - \rho v_{i,j})\delta x = 0 \quad (25)$$

We can solve Eqs. (21)–(25) simultaneously, and then scanning the whole field once or several times point by point to complete one iterative process. These processes are repeated until the iterations are converged. The other variables, such as T, K and ε can be directly solved from Eq. (20).

5.4. Boundary conditions

Solid surfaces: No-slip conditions for velocity were assumed and the turbulent kinetic energy was set to zero on all solid walls. The dissipation of the turbulent kinetic on solid walls had no effect on the internal field because it was obtained from Eq. (12). The two side walls and the upper wall were assumed to be adiabatic. Uniform heat flux was applied to the bottom wall.

Inlet: Profiles of the axial velocity and temperature were assumed to be uniform. The turbulent kinetic energy and its dissipation rate were adopted according to Patankar's method [21].

Outlet: The axial velocity was assumed to match local one-way condition [15]. For the other variables, the Neumann condition was employed.

5.5. The definition of friction factor and Nusselt number

The average friction factor was defined as Eq. (2) and the Nusselt number presented herein was defined as below:

$$Nu = \frac{\int Nu_z \, dz}{\int dz} \tag{26}$$

Nu_z was the local Nusselt number along the main flow direction and given by:

$$Nu_z = \int \left(-\frac{\partial T}{\partial y} \right)_{y=0} dx/(T_W - T_{b,z}) \tag{27}$$

$T_{b,z}$ was the local bulk temperature and defined as:

$$T_{b,z} = \left(\int \int \rho |w| T \, dx \, dy \Big/ \int \int \rho |w| \, dx \, dy \right)_z \tag{28}$$

6. Results and discussion

The average Nusselt number and friction factor of the cross-ribbed rectangular duct obtained from both experimental study and numerical simulation were plotted against angle formed by the cross-ribs and presented in Figs. 3 and 4 respectively.

As seen in Fig. 3, forced convection can be enhanced by mounting cross-ribs on the heated surface of a rectangular duct. The average Nusselt number for the duct with cross-ribbed surface, regardless of the angle, was significantly higher than that for the smooth duct. The findings were in good agreement with those of Wong and Leung [10]. Comparing the thermal performance of the ducts with cross-ribbed surface, the ducts with angle 60° and 70° formed by the cross-ribs produced the highest average Nusselt number. It is obvious that a peak value in the average heat transfer coefficient would be obtained at an angle between 60° and 70°, which is an optimum range corresponding to the maximum forced convection from the ribbed duct to the airflow. In addition, the numerical predictions generally agree with the experimental results in the present study, except that the numerical predictions are on the average slightly lower by 2–10% throughout the entire range of investigation.

When cooler air flows over the electrically heated cross-ribbed surface, development of boundary layer on the surface will be highly affected by the presence of the ribs. Vortex is formed around the rib surface to promote the local turbulence, which will enhance the forced convection. Strength of the vortex depends on several parameters such as the flow condition, the fluid properties and geometry of the ribbed surface, which includes shape and size of the ribs and angle formed by the cross-ribs. The latter also affects directly the separation between adjacent ribs, as it will be reduced when the angle formed by the cross-ribs is increased. Rib separation has been suggested by Han [1] to be an important parameter dominating the thermal performance of a surface with parallel ribs. As the average heat transfer coefficient reduces monotonically when the angle formed by the cross-ribs is increased from 70° to 120°, it is therefore reasonable to suggest that thermal performance of the ribbed duct will continue to decrease when the angle is further increased to 180° (i.e. a parallel-ribbed surface).

Flow fields on the vertical plane at the centerline of the cross-ribbed duct along the main direction airflow were obtained in the present numerical study. The flow field in the ribbed duct, with angle formed by the cross-ribs from 30° to 90°, is shown in Fig. 6. The flow field around the rib surface, including that at the crossing point between two ribs, is presented. At the leeward side of the rib, the streamlines above the duct surface are closer at the angle of 60° or 70°, which implies a higher

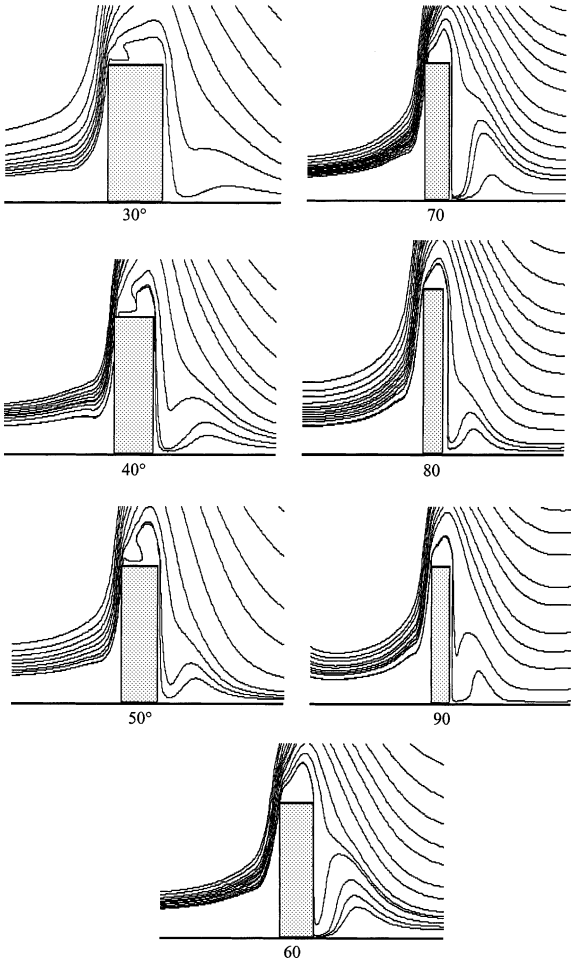

Fig. 6. Local magnified streamlines on the streamwise central plane for various cross-rib angles (a magnification of 10 for the y-axis).

local flow velocity as well as a larger velocity gradient around the wall region. Consequently, it leads to a better promotion of the local turbulence to enhance the secondary flow there and hence results in higher forced convection.

As presented in Fig. 4, the price of enhancing the forced convection by mounting cross-ribs on the internal surface of a rectangular duct is the higher friction factor. A rectangular duct with smooth surface encountered a significantly lower pressure drop than the ducts with ribbed surface. This finding agreed well with the study of Ahn [22], who investigated the effect on forced convection with the use of different rib shapes. Comparing with the experimental results, a slightly higher prediction of 2–11% in the friction factor was obtained from the numerical prediction. Both experimental and numerical simulation studies predicted a maximum friction factor within the range of 70–80°.

7. Conclusions

The present study provided information on the forced convection and pressure drop characteristics of a rectangular duct with its bottom surface mounted with cross-ribs. Such arrangement of ribs has rarely been reported in the literature. Both forced convection and pressure drop in the rectangular duct were enhanced significantly by mounting square-sectioned cross-ribs uniformly on its bottom surface, when it was operating under turbulent flow condition.

According to the present experimental and numerical studies, use of cross-ribs could be a promising solution to enhance the forced convection in a rectangular duct. The ability of the cross-ribbed surface to enhance forced convection was found to be better than the well-known parallel-ribbed surface. The major drawback of applying the cross-ribbed surface was the larger pressure drop and hence a higher friction factor.

An optimum range of angles formed by the cross-ribs corresponding to a maximum enhancement of forced convection was observed. According to the experimental and numerical results obtained, its value would be between 60° and 70°. Within this optimum range, a significantly higher heat transfer coefficient between the ribbed surface and the airflow was obtained.

Acknowledgements

The work described in this paper was fully supported by a grant from the Research Grants Council of the Hong Kong Special Administrative Region (Project No. PolyU5156/99E).

References

[1] J.C. Han, Square channels with parallel, crossed, and V-shaped angled ribs, J. Heat Transfer 113 (1991) 590–596.
[2] T.M. Liou, J.J. Hwang, Effect of ridge shapes on turbulent heat transfer and friction in a rectangular channel, Int. J. Heat Mass Transfer 36 (1993) 931–940.
[3] J.J. Hwang, T.M. Liou, Heat transfer augmentation in a rectangular channel with slit rib-turbulators on two opposite walls, J. Turbomach. 119 (1997) 617–623.
[4] S. Lorenz, D. Mukomilow, W. Leiner, Distribution of heat transfer coefficient in a channel with periodic transverse grooves, Exp. Therm. Fluid Sci. 3 (1995) 234–242.
[5] M. Hwashida, Local heat transfer coefficient distribution on a ribbed surface, Enhanced Heat Transfer 3 (1996) 187–200.
[6] R.P. Saini, J.S. Saini, Heat transfer and friction factor correlations for artificially roughened ducts with expanded metal mesh as roughness element, Int. J. Heat Mass Transfer 40 (4) (1997) 973–986.
[7] P.R. Chandra, M.L. Fontenot, J.C. Han, Effect of rib profiles on turbulent channel flow heat transfer, J. Thermophys. Heat Transfer 12 (1) (1998) 116–118.
[8] L.B. Wang, W.Q. Tao, Q.W. Wang, T.T. Wong, Experimental study of developing turbulent flow and heat transfer in ribbed convergent/divergent square ducts, Int. J. Heat Fluid Flow 22 (2001) 603–613.
[9] C.W. Leung, T.T. Wong, H.J. Kang, Forced convection of turbulent flow in triangular ducts with different angles and surface roughnesses, Heat Mass Transfer 34 (1998) 63–68.
[10] T.T. Wong, C.W. Leung, Forced convection augmentation of turbulent flow in a triangular duct with artificially roughened internal surfaces, Exp. Heat Transfer 15 (2002) 89–106.
[11] J.C. Han, L.R. Glicksman, W.M. Rohsenow, An investigation of heat transfer and friction for rib-roughened surfaces, Int. J. Heat Mass Transfer 21 (1978) 1143–1156.
[12] S.M. Yang, W.Q. Tao, Heat Transfer, third ed., Higher Education Press, Peking, 1998.
[13] W.P. Jones, B.E. Launder, The prediction of laminarization with a two-equation model of turbulence, Int. J. Heat Mass Transfer 15 (1972) 301–314.
[14] M. Wolfshtein, The velocity and temperature distribution in one-dimensional flow with turbulence augmentation and pressure gradient, Int. J. Heat Mass Transfer 12 (1969) 301.
[15] W.Q. Tao, Numerical Heat Transfer, Xi'an Jiaotong University Press, 2001.
[16] S. Chen, T.L. Chan, C.W. Leung, Numerical prediction of laminar forced convection in triangular ducts with unstructured triangular grid method, Numer. Heat Transfer, Part A 38 (2000) 209–224.
[17] P.K. Khosla, S.G. Rubin, A diagonally dominant second order accurate implicit scheme, Comput. Fluids 2 (1974) 207–209.
[18] T. Hayase, J.A.C. Humphery, A.R. Grief, A consistently formulated QUICK scheme for fast and stable convergence using finite volume iterative calculation procedures, J. Comput. Phys. 93 (1992) 108–118.
[19] S.V. Patankar, Numerical Heat Transfer and Fluid Flow, McGraw-Hill, 1980.

[20] S.P. Vanka, Block implicit multigrid solution of the Navier–Stokes equations in primitive variables, J. Comput. Phys. 8 (1986) 417–440.
[21] S.V. Patankar, E.M. Sparrow, M. Ivanovic, Thermal interaction among the confining walls of a turbulent recirculating flow, Int. J. Heat Mass Transfer 24 (1978) 269–274.
[22] S.W. Ahn, The effects of roughness types on friction factors and heat transfer in roughened rectangular duct, Int. Commun. Heat Mass Transfer 28 (7) (2001) 933–942.